



## Understanding the two neutron transfer reaction mechanism in $^{206}\text{Pb}(^{18}\text{O}, ^{16}\text{O})^{208}\text{Pb}$

A. Parmar<sup>a</sup>, Sonika<sup>a</sup>, B.J. Roy<sup>a,\*</sup>, V. Jha<sup>a</sup>, U.K. Pal<sup>a</sup>, T. Sinha<sup>b</sup>,  
S.K. Pandit<sup>a</sup>, V.V. Parkar<sup>a</sup>, K. Ramachandran<sup>a</sup>, K. Mahata<sup>a</sup>, S. Santra<sup>a</sup>,  
A.K. Mohanty<sup>a</sup>

<sup>a</sup> Nuclear Physics Division, Bhabha Atomic Research Centre, Mumbai - 400 085, India

<sup>b</sup> High Energy Nuclear and Particle Physics Division, Saha Institute of Nuclear Physics, Kolkata - 700 064, India

Received 28 January 2015; received in revised form 3 April 2015; accepted 8 April 2015

Available online 16 April 2015

### Abstract

The absolute cross sections for elastic scattering and two-neutron transfer reaction for  $^{18}\text{O} + ^{206}\text{Pb}$  system have been measured at an incident energy near the Coulomb barrier. Detailed coupled reaction channel calculations have been carried out for description of the measured angular distributions for the elastic scattering and transfer reactions simultaneously. The two-neutron transfer reaction  $^{206}\text{Pb}(^{18}\text{O}, ^{16}\text{O})^{208}\text{Pb}$  in the g.s.  $\rightarrow$  g.s. transition is analyzed in (i) extreme cluster model assuming a di-neutron transfer, (ii) two-step successive transfer, and (iii) microscopic approach (independent coordinate scheme) of simultaneous transfer of two neutrons. The relative importance of one step simultaneous transfer versus two-step successive transfer has been studied. Present analysis suggests dominance of cluster transfer of a di-neutron. The contribution from the two-step sequential processes is less significant, however, the combined “two-step plus simultaneous (microscopic)” calculations give a reasonably good agreement with the measurement. The possibility of multi-step route via projectile and target excitations and contribution from such indirect transfer paths to the present two-neutron transfer cross section has been investigated.

© 2015 Elsevier B.V. All rights reserved.

**Keywords:** NUCLEAR REACTIONS  $^{206}\text{Pb}(^{18}\text{O}, ^{18}\text{O})$ ,  $^{206}\text{Pb}(^{18}\text{O}, ^{16}\text{O})$ ,  $E = 79$  MeV; measured  $\sigma(\theta)$ , coupled reaction channel calculations; deduced reaction mechanisms, one- and two-nucleon transfer probabilities

\* Corresponding author.

E-mail address: [bjroy@barc.gov.in](mailto:bjroy@barc.gov.in) (B.J. Roy).

## 1. Introduction

Two-nucleon transfer reactions induced by light and heavy ions are known to be a useful tool for extracting information on nuclear pairing correlations. Extensive studies have been performed and reported in the literature to understand the two-nucleon transfer and pairing effect in nuclei [1–14]. Such studies have received increased impetus due to the availability of neutron rich radio active ion beams where two-neutron transfer reactions are found to be quite dominant [15,16]. In a very recent work, experimental data for the two-neutron transfer are reproduced for the first time in a microscopic calculation by incorporating the nucleon–nucleon pairing correlations [17]. However, it is still an open question whether the information on the pair correlation can be extracted in heavy ion reactions. Studies of single nucleon transfer reactions are of great success in establishing the connection between the cross section and single-particle configuration of the nuclear states, while extraction of structure information from two-nucleon transfer cross section is not straightforward. The complexity increases with heavy ions as multiple transfer paths become possible [18–21] and these possibilities contribute significantly to the absolute cross section. The contribution from a multi-step route involving successive transfer of two single nucleons can be comparable or even higher compared to the one-step direct transfer of correlated nucleons [5,13,22–26]. Moreover, while dealing with heavy ions, one should also take into account the effect of inelastic excitations prior to or after the transfer [11,12,21,27]. The virtual Coulomb excitations in the projectile and/or target can influence the transfer cross section [28] and depending on the projectile and target combination, these effects can be of significant importance. Non-inclusion of these multi-step routes in the transfer reaction analysis could lead to misinterpretation of the experimental results.

Even for single-nucleon transfer reactions, which are usually well described in the DWBA framework using the phenomenological optical-model potential obtained from fitting of elastic scattering data, very often a large normalization factor (so-called unhappiness factor) is invoked to reproduce the absolute magnitude of the experimental cross section. The situation is even worse in the two-nucleon transfer reactions, an arbitrary scaling factor as high as hundred is required to reproduce the experimental angular distributions [12,25,29–31]. Inclusion of successive two-step processes in the calculation improves the discrepancy to some extent [25,31]. In a recent work [1,2] on the two-neutron transfer reaction ( $^{18}\text{O}$ ,  $^{16}\text{O}$ ) on  $^{12}\text{C}$ , the experimental cross sections were reproduced for the first time without the need of any arbitrary normalization and the coupled reaction channel calculations indicated the dominance of one step reaction mechanism for this reaction. This two-nucleon transfer reaction ( $^{18}\text{O}$ ,  $^{16}\text{O}$ ) on various target nuclei has also been studied in the past by several authors [10–13] and different results are obtained. In some of the works the sequential transfer process is found to be dominant over the simultaneous transfer [13] whereas some others observed that the one step process competes strongly with the two-step process [10]. Nevertheless the  $^{18}\text{O}$  induced two-neutron stripping reaction, as mentioned in Ref. [2], is a good candidate for the study of two-nucleon correlations due to the existence of a correlated neutron pair in the  $^{18}\text{O}$  ground state wave function. A systematic exploration of this reaction on different target nuclei would be useful for the study of pairing effects.

In the present work, we have studied the two-nucleon transfer reaction  $^{206}\text{Pb}(^{18}\text{O}, ^{16}\text{O})^{208}\text{Pb}$ . The reaction mechanism has been studied and relative contributions from different processes/transfer paths that are contributing to the absolute cross section have been investigated. The beam energy was chosen at near the Coulomb barrier. For heavy ion transfer reactions around and below the Coulomb barrier the reaction mechanism is less complicated as the effect of attractive nuclear force on the Coulomb trajectory would be minimum and may easily

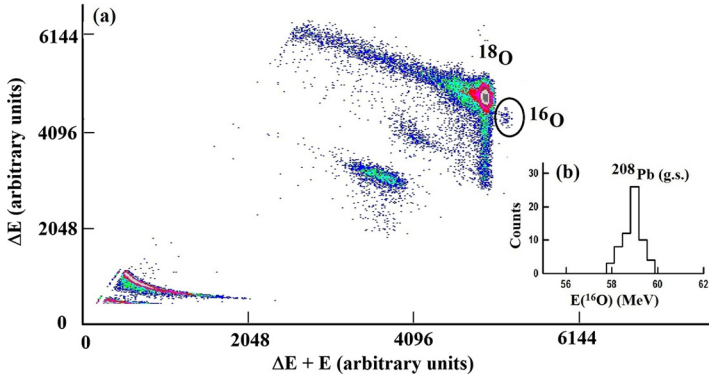


Fig. 1. (Color online.) (a) Typical gain matched  $\Delta E$  vs.  $(\Delta E + E)$  spectrum for the reaction  $^{206}\text{Pb}(^{18}\text{O}, X)$  at  $E(^{18}\text{O}) = 79$  MeV and  $\theta_{lab} = 165^\circ$ . (b)  $x$  projection of  $^{16}\text{O}$  [marked by the circle in (a)]. The peak corresponds to the two-neutron transfer reaction  $^{206}\text{Pb}(^{18}\text{O}, ^{16}\text{O}_{g.s.})^{208}\text{Pb}_{g.s.}$ .

be accounted for. The present two-neutron transfer reaction has the added advantage of having positive Q-value, the Q-value dependence of cross section (optimum Q-value [21]) may favor the population of ground state transition. The reaction calculations are performed using the coupled reaction channel (CRC) formalism. The effect of coupling amongst various reaction channels and relative contributions from direct as well as indirect transfer paths are studied and reaction mechanism has been understood. The paper is organized as follows. The experimental details are given in Section 2. The CRC calculations and results are presented and discussed in Section 3. Analysis in the transfer probability calculations are presented in Section 4. Section 5 deals with the summary and conclusions.

## 2. Experimental details

The measurements are carried out at the BARC – TIFR Pelletron-Linac facility, Mumbai, India. The  $^{18}\text{O}$  ions of energy 79 MeV are used and the target is isotopically enriched  $^{206}\text{Pb}$  (>99%) evaporated on  $^{12}\text{C}$  foil. The target and carbon backing thicknesses are  $250 \mu\text{g}/\text{cm}^2$  and  $30 \mu\text{g}/\text{cm}^2$ , respectively. Reaction products are detected using four silicon surface barrier (SSB) detector telescopes in  $\Delta E - E$  configuration mounted on two movable arms inside the General Purpose Scattering Chamber at  $0^\circ$  beam line of the Pelletron beam hall. Typical thickness of the  $\Delta E$  detectors is  $\sim 25 \mu\text{m}$  and  $E$  detectors are above  $300 \mu\text{m}$ . Each telescope subtended a solid angle of  $\sim 0.5$  msr. Two monitor detectors (SSB detector of thickness 1 mm) are placed at forward angle  $\theta_{lab} = \pm 25^\circ$  with respect to the beam direction for cross section normalization. A good charge and mass resolution has been achieved which allowed the separation of oxygen isotopes from other particles (Fig. 1). Angular distribution for the elastic scattering cross section has been measured in the angular range of  $\theta_{lab} = 85^\circ - 170^\circ$  and the ratio of the elastic scattering cross section to the Rutherford cross section, plotted as a function of centre-of-mass scattering angle, is shown in Fig. 2. The error bars shown in the figure are the statistical uncertainties and in many cases they are within the data symbol. In addition, an overall systematic uncertainty of  $\sim 10\%$  is estimated (mostly for the large angles data) mainly due to the fitting procedure to extract the area under the elastic peak. The angle offset is measured to be  $0.3^\circ$ .

For the two-neutron transfer reaction  $^{206}\text{Pb}(^{18}\text{O}, ^{16}\text{O})^{208}\text{Pb}$ , the ground state of  $^{208}\text{Pb}$  is well separated from the elastic peak due to the positive Q-value ( $Q = +1.917$  MeV) of this reaction

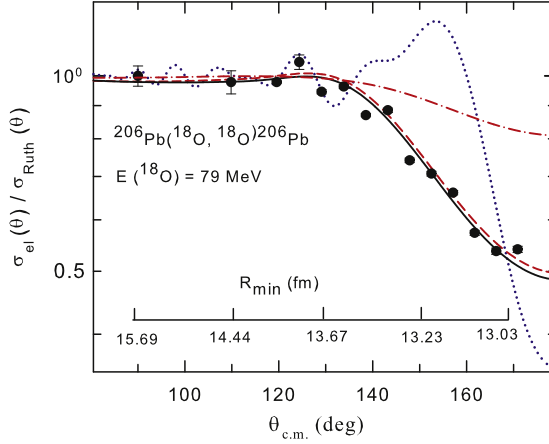


Fig. 2. (Color online.) The reaction calculations along with measured data for the elastic scattering angular distribution in  $^{18}\text{O} + ^{206}\text{Pb}$  at 79 MeV plotted as a ratio to the Rutherford cross section. The results of the FRESKO calculations are shown as i) blue dotted curve when only double-folding potential and short range imaginary potential are considered (no inelastic excitation and no transfer channels are coupled), ii) red dash-dot-dash curve when double-folding potential, short range imaginary and  $^{206}\text{Pb}$  inelastic states are coupled, iii) red dash curve when double-folding potential, short range imaginary and both the target and projectile inelastic excitations are considered and iv) black solid curve when transfer couplings are also included. The definition of  $R_{\min}$ , distance of closest approach, is given later in Section 4.

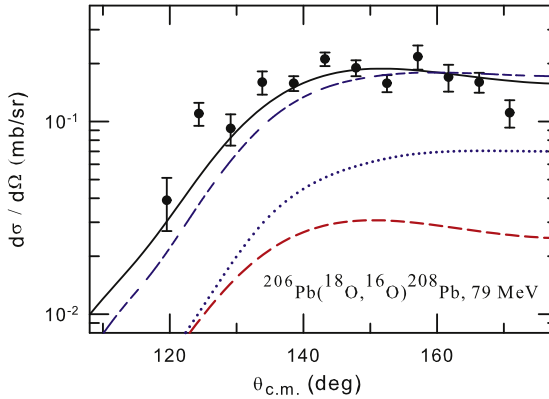


Fig. 3. (Color online.) The measured  $d\sigma/d\Omega$  for the two-neutron transfer reaction  $^{206}\text{Pb}(^{18}\text{O}, ^{16}\text{O}_{g.s.})^{208}\text{Pb}_{g.s.}$  at  $E_{\text{lab}} = 79$  MeV along with the theoretical predictions. The black solid curve is the result from CRC calculations in the extreme cluster model while contribution from the two-step sequential process is shown as blue dotted curve. The results of microscopic calculations for a simultaneous transfer are shown as red dash curve while the curve represented by blue dash (long – short – short) corresponds to the results of combined “two-step (successive) plus one-step (microscopic)” calculations.

and has been clearly identified, as shown in Fig. 1. Angular distribution of cross sections for this two-neutron stripping reaction has been measured and is shown in Fig. 3 along with the error bars. Additionally, a systematic uncertainty in the solid angle measurement is estimated to be  $\sim 3\%$ . The contribution from the carbon backing did not interfere the present data as the maximum angle of  $^{18}\text{O}$  scattering from  $^{12}\text{C}$  is  $\theta_{\text{lab}} \sim 42^\circ$ .

Table 1

Deformation parameters of the  $^{18}\text{O}$  nucleus and experimental  $B(E_\lambda)$  values for the  $2^+$  and  $3^-$  states in  $^{206}\text{Pb}$  nucleus used in the present calculations.

$^{18}\text{O}$						$^{206}\text{Pb}$				
$E_x$ (MeV)	$J^\pi$	$\lambda$	$\delta_\lambda$ (fm)	$\beta_\lambda$	Ref.	$E_x$ (MeV)	$J^\pi$	$\lambda$	$B(E_\lambda)$ ( $e^2\text{b}^{2\lambda}$ )	Ref.
1.982	$2^+$	2	1.25	0.38	[36]	0.803	$2^+$	2	0.10	[37,38]
5.098	$3^-$	3	1.19	0.36	[36]	2.647	$3^-$	3	0.61	[37,38]

### 3. Coupled reaction channel calculations and results

The data are analyzed in the coupled reaction channel model to reproduce, simultaneously, cross sections for the measured elastic scattering and two-neutron transfer reaction. The computer code FRESKO (version FRES 2.9) [32] is used. In the coupling scheme, the elastic scattering, several low lying inelastic excitations in  $^{18}\text{O}$  and  $^{206}\text{Pb}$ , and one- and two-nucleon transfer reactions are included. The one-nucleon transfer includes transition to specific single-particle states in  $^{17}\text{O}$  ( $E_x = 0.0$  MeV,  $5/2^+$ ,  $E_x = 0.871$  MeV,  $1/2^+$  and  $E_x = 3.06$  MeV,  $1/2^-$ ) and single-hole states in  $^{207}\text{Pb}$  ( $E_x = 0.0$  MeV,  $1/2^-$ ;  $E_x = 0.57$  MeV,  $5/2^-$  and  $E_x = 0.89$  MeV,  $3/2^-$ ). The coupling diagram for the two-neutron transfer processes in  $^{206}\text{Pb}(^{18}\text{O}, ^{16}\text{O}_{g.s.})^{208}\text{Pb}_{g.s.}$  is shown in Fig. 4.

The CRC calculations are performed as follows. First, the elastic scattering cross section has been calculated with a bare double folded (DF) real potential. The microscopic double-folding potential  $V_{DF} = \int \int d\mathbf{r}_1 d\mathbf{r}_2 \rho(\mathbf{r}_1) \rho(\mathbf{r}_2) v(\mathbf{r}_{12})$  was computed using the computer program DF-POT [33]. The DF potential consists of folding of a harmonic oscillator density distribution to simulate  $^{18}\text{O}$  with the sum of two Fermi density distributions for the protons and neutrons in  $^{206}\text{Pb}$ . The charge densities are taken from the atomic and nuclear data tables [34] and the M3Y form [35] of the effective nucleon–nucleon interaction  $v(r_{12}) = 7999 \frac{e^{-4r}}{4r} - 2134 \frac{e^{-2.5r}}{2.5r} - 262\delta(r)$  has been used. The calculated elastic scattering angular distribution with this double folding potential reproduces the measured data and no additional scaling to the real part of the potential is needed, as described later.

Next, various non-elastic modes which occur at the nuclear surface are coupled. The absorptive potential is generated through this coupling. For deformation parameters in the projectile  $^{18}\text{O}$  we have used the average experimental values that are listed in Table 1 of Ref. [36] and for the target  $^{206}\text{Pb}$  nucleus, the experimental values that are reported in Refs. [37,38] from the studies of  $^{206}\text{Pb}(^{17}\text{O}, ^{17}\text{O}')$  reaction are used. The values are also listed here in Table 1. The Coulomb and nuclear deformation lengths are taken as equal. The spectroscopic amplitudes (SA) for the one- and two-nucleon transfer reactions, needed to generate the strengths of the various transfer processes concerned in the present study, are taken from the values available in the literature. For the oxygen nuclei we have taken the values from a recent work of Cavallaro et al., [2]. For Pb nuclei the values that are reported in Refs. [39–41] have been used. The amplitudes are also listed in Table 2 here. The two-neutron stripping channel includes a one-step simultaneous transfer and two-step successive transfer. The sequential transfer involves various intermediate states as shown in the coupling diagram (Fig. 4). The details of the transfer calculations are described later.

In addition, as explained in Ref. [26], a short range imaginary potential of Woods Saxon type with  $V_0 = 40$  MeV,  $r_0 = 1.0$  fm and  $a_0 = 0.4$  fm is used. An absorption cross section of  $\sim 23$  mb

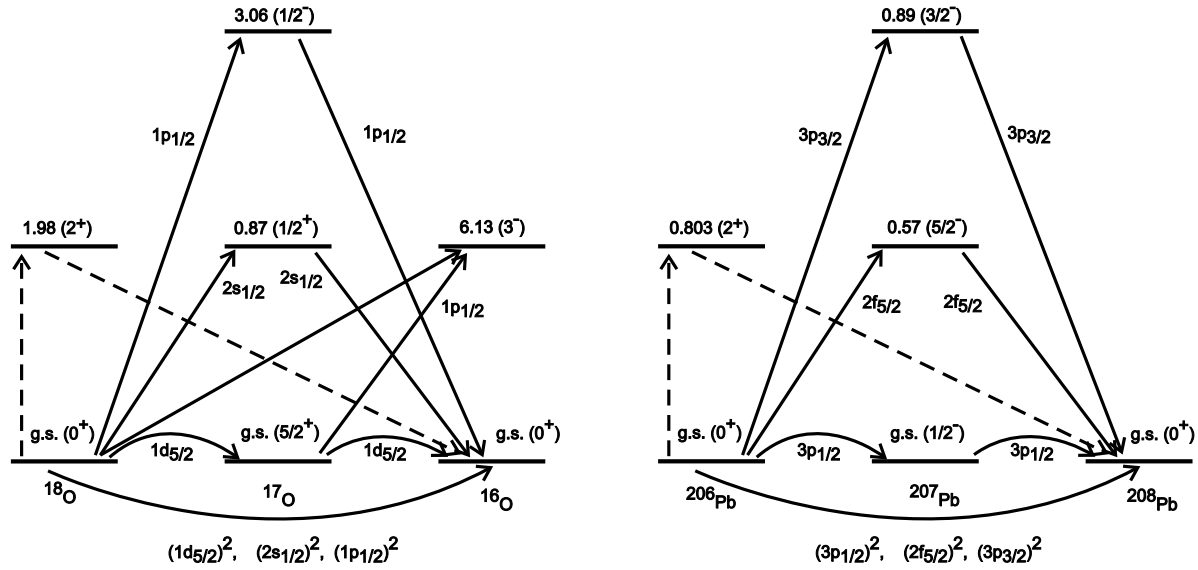


Fig. 4. Coupling diagram showing different transfer paths (direct and two-step) used in the calculation for the present two-neutron transfer reaction. The levels in  $^{17}\text{O}$  and  $^{207}\text{Pb}$  concerned in the sequential transfer are  $d_{5/2}$ ,  $s_{1/2}$  and  $p_{1/2}$  single-particle states and  $p_{1/2}$ ,  $f_{5/2}$  and  $p_{3/2}$  single-hole states, respectively. Coupling of the inelastic excitation ( $2^+$  state) in the projectile and target that are shown here are done for the calculations carried out at the later stage when contributions from the indirect transfer paths through virtual excitations are studied.

Table 2

Spectroscopic amplitudes (SA) for various one- and two-nucleon transfers used in the present calculations. The values for the light nuclei (oxygen isotopes) are taken from a recent work of Cavallaro et al., [2] and that for Pb isotopes are taken from the Refs. [39–41].

	nlj	SA		nlj	SA
$^{18}\text{O}(0^+) \rightarrow ^{17}\text{O}(5/2^+)$	$1d_{5/2}$	+1.305	$^{18}\text{O}(0^+) \rightarrow ^{16}\text{O}(0^+)$	$(1d_{5/2})^2$	-0.871
$^{18}\text{O}(0^+) \rightarrow ^{17}\text{O}(1/2^+)$	$2s_{1/2}$	+0.566		$(2s_{1/2})^2$	-0.367
$^{18}\text{O}(0^+) \rightarrow ^{17}\text{O}(1/2^-)$	$1p_{1/2}$	-0.929		$(1p_{1/2})^2$	+0.241
$^{17}\text{O}(5/2^+) \rightarrow ^{16}\text{O}(0^+)$	$1d_{5/2}$	+0.972	$^{18}\text{O}(0^+) \rightarrow ^{16}\text{O}(3^-)$	$(1p_{1/2}1d_{5/2})$	+0.801
$^{17}\text{O}(1/2^+) \rightarrow ^{16}\text{O}(0^+)$	$2s_{1/2}$	+0.975	$^{206}\text{Pb}(0^+) \rightarrow ^{208}\text{Pb}(0^+)$	$(3p_{1/2})^2$	+0.769
$^{17}\text{O}(5/2^+) \rightarrow ^{16}\text{O}(3^-)$	$1p_{1/2}$	-0.718		$(2f_{5/2})^2$	+0.477
$^{206}\text{Pb}(0^+) \rightarrow ^{207}\text{Pb}(1/2^-)$	$3p_{1/2}$	+0.720	$^{206}\text{Pb}(2^+) \rightarrow ^{208}\text{Pb}(0^+)$	$(3p_{3/2})^2$	+0.426
$^{206}\text{Pb}(0^+) \rightarrow ^{207}\text{Pb}(5/2^-)$	$2f_{5/2}$	+0.368		$(3p_{1/2}2f_{5/2})$	+0.724
$^{206}\text{Pb}(0^+) \rightarrow ^{207}\text{Pb}(3/2^-)$	$3p_{3/2}$	+0.546		$(3p_{1/2}3p_{3/2})$	-0.523
$^{207}\text{Pb}(1/2^-) \rightarrow ^{208}\text{Pb}(0^+)$	$3p_{1/2}$	+0.957		$(2f_{5/2})^2$	+0.278
$^{207}\text{Pb}(5/2^-) \rightarrow ^{208}\text{Pb}(0^+)$	$2f_{5/2}$	+0.861			
$^{207}\text{Pb}(3/2^-) \rightarrow ^{208}\text{Pb}(0^+)$	$3p_{3/2}$	+0.875			

for the fusion channel has been obtained from the present calculation which is slightly higher than the measured fusion cross section for the  $^{16}\text{O} + ^{208}\text{Pb}$  reaction at about the same centre-of-mass energy [42]. The sensitivity of the fusion cross section to this short range absorptive potential has been studied. A set of CRC calculations have been performed in which the diffuseness parameter is reduced from 0.4 fm to 0.2 fm. The fusion cross section is almost insensitive on the choice of this potential by varying  $a_0$  from 0.4 fm to 0.2 fm while a change in the radius parameter  $r_0$  from 1.0 fm to 1.2 fm leads to a decrease in the fusion cross section by  $\sim 10\%$ .

The results of the present CRC calculations for the elastic scattering angular distribution are shown in Fig. 2 and are compared with the experimental data. From the calculations it has been observed that the elastic and inelastic channels are strongly coupled. For the elastic scattering angular distribution, the inclusion of inelastic excitations in the CRC calculations has significant effects at larger angles (Fig. 2). It has been observed, as can be seen in the figure, that the effect due to the coupling of the  $2^+$  ( $E_x = 1.98$  MeV) state of  $^{18}\text{O}$  is significant on the elastic scattering angular distribution while the target excitation ( $2^+$  state at 0.803 MeV) has relatively less influence. It is to mention that the  $2^+$  state of  $^{206}\text{Pb}$  has relatively low deformation parameter  $\beta_2 = 0.03$  (calculated from the  $B(E2)$  value reported in [37,38] with  $R = 1.25 \times A^{1/3}$  fm) as compared to the  $\beta_2$  value [36] of 0.38 for the first excited  $2^+$  state in  $^{18}\text{O}$  which might be the possible reason. The inclusion of transfer channels is observed to have little effect on the elastic scattering cross section. Overall agreement between the calculation and the measured data, after inclusion of all these channels, is reasonably good.

The calculations of two-neutron transfer reaction cross sections are performed with an emphasis to understand the relative importance of various processes that governs the transfer mechanism. The transfer calculations are done in the (i) extreme cluster model assuming a di-neutron transfer, (ii) microscopic consideration of the two-nucleon simultaneous transfer and (iii) two-step successive transfer. In the extreme cluster model, the two neutrons are assumed to be spatially correlated. The  $2n$  cluster is assumed to be in the  $S = 0$  and  $T = 1$  state and the  $1s$  internal motion for the cluster is considered [35]. The interaction potential is assumed to act on the centre-of-mass of the correlated neutron pair. Under this assumption, the transfer is described

in the similar way as that for a single-nucleon. The quantum numbers ( $N, L$ ) of the centre-of-mass motion are calculated using the harmonic-oscillator energy conservation relation as given in Ref. [35]

$$2(N - 1) + L + 2(n - 1) + 1 = \sum_{i=1}^2 2(n_i - 1) + l_i,$$

where  $(n_i, l_i)$  are the quantum numbers of the individual transferred nucleons. The initial and final bound state wavefunctions for the di-neutron are generated in a Woods Saxon potential well with the parameters  $r_0 = 1.2$  fm and  $a_0 = 0.58$  fm and the depth of the well is adjusted to reproduce the two-neutron separation energy. The finite range transfer calculations are carried out with the post form of the interaction potential including the full complex remnant term. The spectroscopic amplitude for the di-neutron cluster is taken as 1.0. In the present calculations, the  $N = 3, L = 0$  configuration is used for the cluster in the  $^{18}\text{O}$  ground state. The contribution from the other  $N = 2, L = 0$  configuration with amplitude 0.241 is observed to be less important.

The successive transfer calculations are performed as follows. In the shell model description, the ground state of  $^{206}\text{Pb}$  is described as [40] two-particle hole with respect to the  $N = 126$  core and can be written as

$$\psi_{g.s.} = 0.769(3p_{1/2})^0 + 0.477(2f_{5/2})^4 + 0.426(3p_{3/2})^2.$$

Thus, in the description of sequential processes for the transition  $^{206}\text{Pb}(0^+) \rightarrow ^{208}\text{Pb}(0^+)$ , three intermediate channels populating the  $1/2^-$  (g.s.),  $5/2^-$  (1<sup>st</sup> excited state) and  $3/2^-$  (2<sup>nd</sup> excited state) in  $^{207}\text{Pb}$  are considered (see Fig. 4). Similarly, in the shell model calculations of Ref. [2] using the  $1p_{1/2}, 1d_{5/2}$  and  $2s_{1/2}$  model space, the ground state wavefunction for  $^{18}\text{O}$  nucleus (two-particle state above the  $^{16}\text{O}$  core) is described as

$$\psi_{g.s.} = -0.871(1d_{5/2})^2 - 0.367(2s_{1/2})^2 + 0.241(1p_{1/2})^2.$$

Therefore, successive paths for the transition  $^{18}\text{O}(\text{g.s.}) \rightarrow ^{16}\text{O}(\text{g.s.})$  involve three intermediate channels that populate the  $5/2^+$  (g.s.) and  $1/2^+$  (1<sup>st</sup> excited state) and  $1/2^-$  (2<sup>nd</sup> excited state) in  $^{17}\text{O}$  nucleus. In this model of two-step transfer of single-nucleons, the interaction potential acts twice and the form factors are calculated by incorporating the appropriate one-neutron separation energies. The reaction calculations are done in the prior-post combination to avoid the non-orthogonality terms [32].

The results of the extreme cluster model and successive transfer are shown in Fig. 3. The di-neutron cluster model calculation reproduces reasonably well the observed two-nucleon transfer cross section both in shape and absolute magnitude. No arbitrary normalization – the so-called unhappiness factor that usually requires to reproduce transfer cross section is needed. The cluster cross section is usually sensitive on the choice of binding well parameters, the dependence of the cross section on the radius ( $r_0$ ) and diffuseness ( $a_0$ ) parameters has been investigated. A set of CRC calculations are carried out in which the  $r_0$  and  $a_0$  are varied. A change in radius from  $R = 1.2 \times A^{1/3}$  fm to  $1.25 \times A^{1/3}$  fm for both the projectile and residual nucleus leads to an increase in the cross section by a factor of  $\sim 2$  while the cross section goes down by about the same factor when the radius reduces to  $1.15 \times A^{1/3}$ . The variation in the diffuseness parameter has somewhat less effect on the cross section. An increase (decrease) in  $a_0$  from 0.6 fm to 0.65 (0.55) fm increases (decreases) the cross section by a factor  $\sim 1.5$ .

The agreement between the measured two-neutron stripping cross section and calculations involving two-step sequential processes differ significantly with the latter underestimating the measurement. The agreement with the shape of the angular distribution is also not that satisfactorily especially at the extreme backward angles where the predictions show an increasing trend while the experimental data shows a small decreasing behavior. The present calculations suggest the cluster transfer as the dominant mechanism over the successive transfer.

We have also carried out a detailed microscopic calculations for the simultaneous transfer of two neutrons. In the microscopic approach [35] (the so-called independent coordinate scheme), the two nucleons are not restricted to be in the 1s internal motion and the transition potential is assumed to act separately on each of the transferred nucleons. The overlaps/two-nucleon form factors are then evaluated microscopically by transforming the two single-particle eigenfunctions of a Wood Saxon potential well. The single-nucleon radial wave functions are evaluated using the same well geometry ( $r_0 = 1.2$  fm and  $a_0 = 0.6$  fm) and the half-separation energy procedure is used to fix the well depths. The choice of half of the two-neutron separation energy, which ignores any mutual potential energy due to the residual interaction, seems reasonable in the present case of weakly interacting neutron pair. The two-particle form factors are calculated in the post form of the interaction potential with the prior form of the potential giving similar results. The two-particle spectroscopic amplitudes used in the present calculations are listed in Table 2. The adopted coupling schemes are sketched in Fig. 4.

The CRC results of the microscopic calculations for the two-neutron transfer are shown in Fig. 3. The shape of the angular distribution seems reasonably agreeing with the measurement, however, the discrepancy in the absolute magnitude is large. Contribution from the two step successive calculations is higher in magnitude than the microscopic ones especially at larger angles but the predicted values from both these calculations are lower than the experimental measurement. The combined “two-step (successive) plus one-step (microscopic)” calculations have also been performed. As can be seen from the results in Fig. 3, the one-step plus two-step calculations give a good description of the order of magnitude of the experimental cross section though some disagreement in the shape of the angular distribution is observed. It should be mentioned that the inverse pick-up reaction  $^{208}\text{Pb}(^{16}\text{O}, ^{18}\text{O})^{206}\text{Pb}$  has been studied earlier by Franey et al., [43] at bombarding energies around the Coulomb barrier and a detailed analysis for the 86 MeV data (slightly above the Coulomb barrier) is reported in Ref. [39]. In that analysis of Bayman et al. [39], direct one-step and two-step sequential transfers were investigated in the first-plus-second order Born approximation. It was observed that the second-order Born approximation terms contribute most of the transition amplitude while contribution from the first-order Born approximation was poor. The overall conclusion in that paper was that the transfer of two neutrons occurs predominantly by a successive transfer mechanism with the two-step processes account for almost all the observed cross section and contribution from the one-step simultaneous transfer is less important. Though the multi-step sequential processes are usually dominant reaction mechanism in transfer reactions between heavy ions, however, there are examples where the direct transfer of a correlated two-nucleon pair is equally important (Refs. [1,10] and the references therein). In Ref. [1] it was observed that the direct DWBA calculations using the Fresco code reproduces the order of magnitude of the measured cross section for  $^{18}\text{O} + ^{12}\text{C} \rightarrow ^{16}\text{O} + ^{14}\text{C}_{g.s.}$  transition while the sequential transfer underestimates the experimental cross section even of one order of magnitude at large angles. The calculations with the coherent sum of the amplitudes of the direct and sequential processes in that reaction showed the importance of interference between the two processes in describing the experimental differential cross section.

The coupled reaction channel analysis of the present data and the calculations in the combined “successive plus direct” transfer might be indicating the role of such interference effect.

The present calculations in the independent particle scheme yielded smaller cross section in comparison with the predictions from the extreme cluster model. Though the two nucleon wave functions can be ideally described both in the cluster and independent particle basis representations but the reason behind the difference in the two results, as mentioned in Ref. [2], could be that the model space used in the microscopic calculations are limited and that more number of pairs of single particle wavefunctions might be necessary to describe the cluster structure. Recent shell model calculations for oxygen isotopes involving more larger model space (full p-s-d space [44]) and (p-sd-pf space [45]) are available, however, such calculations are not performed in the present work. It is also to mention that the extreme cluster model is a more simplistic approach where only the component with the two neutrons coupled antiparallel to a zero intrinsic angular momentum ( $S = 0$ ) participates in the transfer and the interaction depends only on the position of the centre of mass of the cluster and not on its internal variables [35]. Therefore the discrepancy between the two results, as mentioned in Ref. [30], is not very surprising as the two treatments calculate the two-nucleon form factors differently.

We have also studied the effect of indirect transfer paths via virtual excitations in the projectile and target. The contributions from such indirect paths in the two-neutron transfer reaction  $^{206}\text{Pb}(^{18}\text{O}, ^{16}\text{O})^{208}\text{Pb}$  are calculated. The following inelastic excitations in the projectile and target nuclei are added in the coupling diagram as shown in Fig. 4, (i) projectile excitation ( $2^+$  state at  $E_x = 1.98$  MeV) and (ii) target excitation (first excited  $2^+$  state at  $E_x = 0.803$  MeV). The calculations for the present two-neutron transfer reaction are then carried out with the inclusion of these two virtual excitations. For the two nucleon spectroscopic amplitude of the overlap  $\langle ^{18}\text{O}(2^+) | ^{16}\text{O}_{g.s.} \rangle$ , we have taken the value  $SA = -0.324$  that is given in Ref. [12] from BCS-RPA calculations with the two neutrons in oxygen system in  $(sd)^2$  configurations. In an earlier work [11] on this two nucleon stripping reaction ( $^{18}\text{O}, ^{16}\text{O}$ ) on Germanium target it was observed that the calculations with a unit spectroscopic amplitude for this  $^{18}\text{O}(2^+)$  state could not reproduce the experimental data, a value of  $-0.32$  was needed to describe the data. Later in the BCS calculations [12] it was shown that the spectroscopic amplitude of the  $J = 2$  transfer is  $-0.324$ . The present CRC calculations are performed with this value of the spectroscopic amplitude. The SA for  $2^+$  state in  $^{206}\text{Pb}$  nucleus (overlap of  $\langle ^{208}\text{Pb}_{g.s.} | ^{206}\text{Pb}(2^+) \rangle$ ) are taken from shell model calculated values from Ref. [40].

The results of the present CRC calculations for the two-neutron stripping reaction including these virtual excitations are displayed in Fig. 5. As can be seen in the figure, the effect of projectile excitation in the microscopic calculations is to reduce the cross section by about 15% at large angles while the effect of this  $^{18}\text{O}$  excitation on the results of the combined “simultaneous plus successive” calculations is somewhat less (a reduction in the absolute cross section by  $\sim 7\%$ ). Inclusion of the target excitation is observed to alter the transfer cross section very little and hence are not shown in the figure.

We have also carried out the calculations in the extreme cluster model taking into account the indirect transfer paths. As stated above, the value of SA for the overlap  $\langle ^{18}\text{O}(2^+) | ^{16}\text{O}_{g.s.} \rangle$  was taken as  $-0.324$ . The calculations performed in this model with unit spectroscopic amplitude for the di-neutron cluster in the ground state is observed (as shown by black dotted curve in Fig. 5) to overestimate the experimental data at large angles. Calculations with a reduced value of  $SA = 0.85$  give somewhat better agreement with the measurement (black solid curve in Fig. 5).

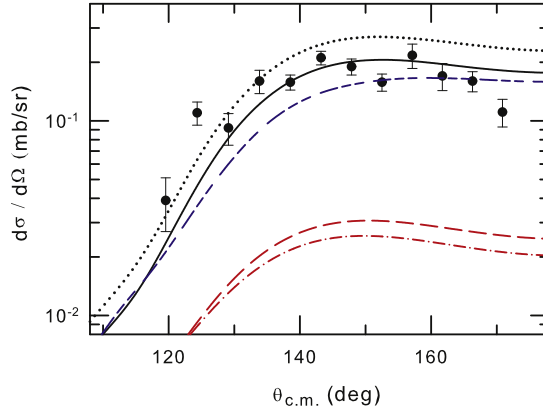


Fig. 5. (Color online.) The CRC calculations for the two-neutron transfer cross section showing the effect of indirect transfer path via virtual excitations in the projectile. The microscopic calculations for a simultaneous transfer and the results after inclusion of the indirect transfer path via projectile excitation are shown as red dash (long dash) curve and red dash–dot–dash curve, respectively. The results of combined “two-step (successive) plus one-step (microscopic)” calculations with the inclusion of the indirect transfer path via the  $^{18}\text{O}$  ( $2^+$  state) are shown as blue dash (long – short – short) curve. The extreme cluster model calculations with the inclusion of the projectile excitation are shown as black dotted curve assuming  $SA = 1$  for the di-neutron cluster in the ground state while the black solid curve is the results with  $SA = 0.85$ .

#### 4. Analysis in terms of transfer probability

The present two-nucleon transfer reaction  $^{206}\text{Pb}(^{18}\text{O}, ^{16}\text{O})^{208}\text{Pb}$  has also been analyzed in the transfer probability approach [18,46,47]. The transfer probability,  $P_{tr}$ , is usually defined as the ratio of transfer cross section to the elastic cross section both measured simultaneously. The two-nucleon transfer probability ( $P_{2n}$ ), in the absence of any pairing correlation between the transferred nucleons, would be equal [46,48] to the product of two independent single-nucleon transfer probability ( $P_{1n}$ )<sup>2</sup>. Thus, an enhancement factor (EF) can be defined as the ratio of  $P_{2n}$  over ( $P_{1n}$ )<sup>2</sup> and would be an indicative of the importance of interaction responsible for correlated pair transfer, if any. This may be a simplified model as is described in Ref. [17], however, a large enhancement factor would be indicative of the dominance of one-step cluster transfer over the two-step sequential processes [48,49]. The transfer probabilities are usually expressed as a function of the distance of closest approach ( $R_{min}$ ) and the distance of closest approach can be calculated [18], assuming a pure Coulomb trajectory, as

$$R_{min} = \frac{Z_p Z_t e^2}{2E_{c.m.}} \left( 1 + \frac{1}{\sin\left(\frac{\theta_{c.m.}}{2}\right)} \right).$$

The notations have their usual meaning. The values of  $R_{min}$  have been calculated using this expression. In the present near-Coulomb barrier energy, the correction in  $R_{min}$  due to the attractive nuclear potential is small and is not considered.

The two-neutron transfer probabilities deduced from the present experimental data are shown in Fig. 6 along with the probabilities for the single neutron stripping. For the  $1n$ -transfer reaction, transition to single hole states  $3p_{1/2}$ ,  $2f_{5/2}$  and  $3p_{3/2}$  are considered and the corresponding cross sections are taken from the calculated values. The two-neutron stripping involves the transition  $^{206}\text{Pb}(g.s.) \rightarrow ^{208}\text{Pb}(g.s.)$  and, as mentioned above, the ground state has 59% of  $[(3p_{1/2})^2]$  con-

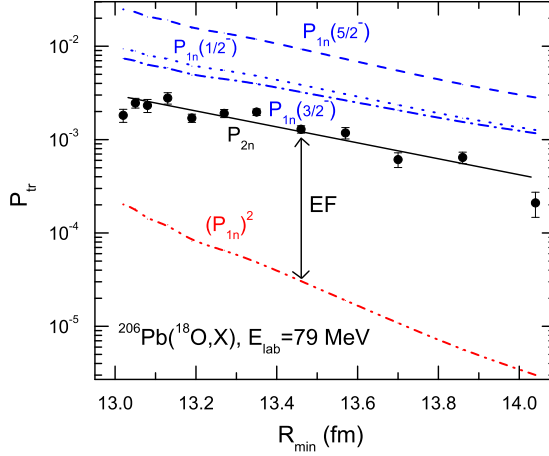


Fig. 6. (Color online.) The transfer probabilities for the single- and two-nucleon stripping reactions plotted as a function of the distance of closest approach  $R_{min}$ . The  $P_{2n}$  is derived from the present experimental data while for  $P_{1n}$  to various single particle states in  $^{207}\text{Pb}$ , the calculated transfer cross sections are used and are shown as i) blue dotted line for transitions to the  $1/2^-$  state, ii) blue dashed line for transitions to the  $5/2^-$  state and iii) blue dash–dot–dash line for transitions to the  $3/2^-$  state. The expression used to calculate  $(P_{1n})^2$ , shown as dash–dot–dot–dash line (red), is given in the text. The black solid line drawn through the data points of  $P_{2n}$  is merely to guide the eye.

figuration, 23% of  $[(2f_{5/2})^2]$  configuration and 18% of  $[(3p_{3/2})^2]$  configuration. Therefore, the enhancement factor for the population of the ground state ( $0^+$ ) of  $^{208}\text{Pb}$  by a pair of neutrons is

$$EF = \frac{P_{2n}(g.s.(0^+) \rightarrow g.s.(0^+))}{0.59 \times (P_{1n})^2\{1/2^-\} + 0.23 \times (P_{1n})^2\{5/2^-\} + 0.18 \times (P_{1n})^2\{3/2^-\}}.$$

As seen in Fig. 6, a significant enhancement of the  $2n$  transfer probability, by more than an order of magnitude, is observed. The enhanced transfer probability seems to suggest that the reaction mechanism prefers to proceed through a transfer of correlated neutron pair than through successive transfer of two neutrons.

## 5. Summary and conclusion

The angular distributions of elastic scattering and two-neutron transfer reaction for the  $^{18}\text{O} + ^{206}\text{Pb}$  system have been measured at near the Coulomb barrier energy of  $E(^{18}\text{O}) = 79$  MeV. The data have been analyzed simultaneously for the elastic scattering and two-nucleon transfer angular distribution in the coupled reaction channel formalism. CRC calculations using the code FRESKO have been performed by coupling the elastic scattering channel, several low lying inelastic excitations in the projectile and target nuclei, and one- and two-neutron transfer reactions. The double folding real potential has been used and a short range absorptive potential is added. The two-neutron transfer reaction  $^{206}\text{Pb}(^{18}\text{O}, ^{16}\text{O}_{g.s.})^{208}\text{Pb}_{g.s.}$  has been studied in detail and the underlying reaction mechanism is investigated. The present calculations in the extreme cluster model assuming a di-neutron transfer and with the microscopic double-folded potential are successful in describing the observed angular distributions for the two-neutron transfer and elastic scattering angular distribution, simultaneously, without the need of any arbitrary scaling factor. The analysis of the present data in terms of transfer probability also suggests the dominance of a one-step cluster transfer over the uncorrelated transfer of two neutrons.

Predictions from the two-step successive transfer alone dominant over the one-step microscopic calculations but the results from both these calculations underpredict the absolute differential cross section of the experimental data. The combined “two-step plus one-step” calculations give an overall good agreement with the measurement.

The effect of indirect transfer paths involving inelastic excitations in the projectile and target nuclei has also been investigated. The calculations in the extreme cluster model taking into account the indirect transfer paths indicate the necessity to use slightly smaller value of the spectroscopic amplitude than 1.0 that is usually assume for this model. The projectile excitation ( $2^+$  state at  $E_x = 1.98$  MeV) is observed to have a sizeable effect on the present two-neutron transfer differential cross section. Such multi-step processes may tend to obscure the sensitivity of multi-particle correlations, a detailed analysis is required in which the various alternative paths and their interferences are considered explicitly. The contributions from all such processes must be taken into consideration for understanding of the reaction mechanism aspects and to extract any information on the pairing interaction.

## Acknowledgements

The excellent support of the operation staff of the BARC-TIFR Pelletron-Linac facility, Mumbai is highly appreciated. We would also like to thank the staff of the target laboratory, TIFR for preparation of the target. The authors are grateful to the Research Centre, Juelich for providing us enriched  $^{206}\text{Pb}$  target material. We would like to thank Dr. E.T. Mirgule, Dr. V. Nanal, Dr. A. Srivastava, Dr. R. Palit, Mr. A.B. Parui, Mr. P. Patale and Mr. R. Kujur for their help during the experiment.

## References

- [1] M. Cavallaro, F. Cappuzzello, M. Bondi, D. Carbone, V.N. Garcia, A. Gargano, S.M. Lenzi, J. Lubian, C. Agodi, F. Azaiez, M. De Napoli, A. Foti, S. Franchoo, R. Linares, D. Nicolosi, M. Niikura, J.A. Scarpaci, S. Tropea, EPJ Web Conf. 66 (2014) 03017.
- [2] M. Cavallaro, F. Cappuzzello, M. Bondi, D. Carbone, V.N. Garcia, A. Gargano, S.M. Lenzi, J. Lubian, C. Agodi, F. Azaiez, M. De Napoli, A. Foti, S. Franchoo, R. Linares, D. Nicolosi, M. Niikura, J.A. Scarpaci, S. Tropea, Phys. Rev. C 88 (2013) 054601.
- [3] G. Potel, A. Idini, F. Barranco, E. Vigezzi, R.A. Broglia, Rep. Prog. Phys. 76 (2013) 106301.
- [4] Ilyas Inci, Andrea Vitturi, J. Phys. Conf. Ser. 321 (2011) 012004.
- [5] L. Corradi, G. Pollarolo, S. Szilner, J. Phys. G, Nucl. Part. Phys. 36 (2009) 113101.
- [6] W. von Oertzen, A. Vitturi, Rep. Prog. Phys. 64 (2001) 1247.
- [7] R.A. Broglia, C.H. Dasso, S. Landowne, B.S. Nilsson, A. Winther, Phys. Lett. B 73 (1978) 401.
- [8] D.M. Brink, R.A. Broglia, Nuclear Superfluidity: Pairing in Finite Systems, Cambridge University Press, Cambridge, England, 2005.
- [9] R.A. Broglia, V. Zelevinsky, Fifty Years of Nuclear BCS – Pairing in Finite Systems, World Scientific, Singapore, 2013.
- [10] T. Takemasa, H. Yoshida, Nucl. Phys. A 304 (1978) 229.
- [11] P.D. Bond, H.J. Kerner, M.-C. Lemaire, D.J. Pisano, C.E. Thorn, Phys. Rev. C 16 (1977) 177.
- [12] M.-C. Lemaire, K.S. Low, Phys. Rev. C 16 (1977) 183.
- [13] T. Kammuri, Nucl. Phys. A 259 (1976) 343.
- [14] J.F. Petersen, D.A. Lewis, D. Dehnhard, H.P. Morsch, B.F. Bayman, Phys. Rev. Lett. 36 (1976) 307.
- [15] A. Chatterjee, et al., Phys. Rev. Lett. 101 (2008) 032701.
- [16] I. Tanihata, et al., Phys. Rev. Lett. 100 (2008) 192502.
- [17] D. Montanari, et al., Phys. Rev. Lett. 113 (2014) 052501.
- [18] C.Y. Wu, W. von Oertzen, D. Cline, M.W. Guidry, Annu. Rev. Nucl. Part. Sci. 40 (1990) 285.
- [19] K.E. Rehm, Annu. Rev. Nucl. Part. Sci. 41 (1991) 429.

- [20] A.M. Stefanini, G. Nebbia, S. Lunardi, G. Montagnoli, A. Vitturi, in: Proceedings of the International Workshop on Heavy-Ion Fusion: Exploring the Variety of Nuclear Properties, 1994, Padova (Italy), World Scientific, Singapore, 1995.
- [21] R. Bass, Nuclear Reactions with Heavy Ions, Springer Verlag, 1980.
- [22] R.A. Broglia, U. Götz, M. Ichimura, T. Kammuri, A. Wirthner, Phys. Lett. B 45 (1973) 23.
- [23] T. Kammuri, Phys. Lett. B 51 (1974) 442.
- [24] E. Maglione, G. Pollarolo, A. Vitturi, R.A. Broglia, A. Winther, Phys. Lett. B 162 (1985) 59.
- [25] P.P. Tung, K.A. Erb, M.W. Sachs, G.B. Sherwood, R.J. Ascutto, D.A. Bromley, Phys. Rev. C 18 (1978) 1663.
- [26] V. Jha, B.J. Roy, A. Chatterjee, H.S. Patel, B. Srinivasan, M.G. Betigeri, H. Machner, Eur. Phys. J. A 15 (2002) 389.
- [27] Norman K. Glendenning, Georg Wolsching, Phys. Rev. Lett. 34 (1975) 1642.
- [28] R.H. Morf, K. Adler, Helv. Phys. Acta 45 (1972) 1094.
- [29] M.C. Mermaz, A. Greiner, B.T. Kim, M.A.G. Fernandes, N. Lisbona, E. Müller, W. Chung, B.H. Wildenthal, Phys. Rev. C 20 (1979) 2130.
- [30] Y. Eisen, H.T. Fortune, W. Henning, D.G. Kovar, S. Vigdor, B. Zeidman, Phys. Rev. C 13 (1976) 699.
- [31] R.E. Rehm, B. Glagola, W.C. Ma, W. Phillips, F.L.H. Wolfs, Z. Phys. A 340 (1991) 281.
- [32] I.J. Thompson, Comput. Phys. Rep. C 7 (1988) 167, <http://www.fresco.org.uk>.
- [33] J. Cook, Comput. Phys. Commun. 25 (1982) 125.
- [34] H. De Vries, C.W. De Jager, C. De Vries, At. Data Nucl. Data Tables 36 (1987) 495.
- [35] G.R. Satchler, Direct Nuclear Reactions, Clarendon Press, Oxford University Press, 1983.
- [36] A.A. Rudchik, et al., Nucl. Phys. A 785 (2007) 293.
- [37] F.G. Knodev, Nucl. Data Sheets 109 (2008) 1527.
- [38] D.J. Horen, et al., Phys. Rev. C 44 (1991) 128.
- [39] B.F. Bayman, Jongsheng Chen, Phys. Rev. C 26 (1982) 1509.
- [40] W.W. True, Phys. Rev. 168 (1968) 1388.
- [41] P.J. Ellis, T. Engeland, Nucl. Phys. A 144 (1970) 161.
- [42] C.R. Morton, A.C. Berriman, M. Dasgupta, D.J. Hinde, J.O. Newton, K. Hagino, I.J. Thompson, Phys. Rev. C 60 (1999) 044608.
- [43] M.A. Franey, B.F. Bayman, J.S. Lilley, W.R. Phillips, Phys. Rev. Lett. 41 (1978) 837.
- [44] C. Yuan, T. Suzuki, T. Otsuka, F. Xu, N. Tsunoda, Phys. Rev. C 85 (2012) 064324.
- [45] M. Bouhelal, F. Haas, E. Caurier, F. Nowacki, A. Bouldjedri, Nucl. Phys. A 864 (2011) 113.
- [46] W. von Oertzen, in: C. Detraz, P. Kienle (Eds.), Proc. Int. School on Physics: “Enrico Fermi”, 1991.
- [47] W. von Oertzen, H.G. Bohlen, B. Gebaur, R. Kuenkel, F. Puehhofer, D. Schuell, Z. Phys. A 326 (1987) 463.
- [48] M. Evers, M. Dasgupta, D.J. Hinde, D.H. Luong, R. Rafiei, R. du Rietz, Phys. Rev. C 84 (2011) 054614.
- [49] B.J. Roy, B. Srinivasan, E. Shallom, M.G. Betigeri, H.C. Jain, M.L. Jhingan, Nucl. Phys. A 588 (1995) 706.